Published in final edited form as:
J Nucl Med. 2017 January ; 58(1): 156–161. doi:10.2967/jnumed.116.177519.

[^{18}F]Fluorosulfate for PET imaging of the sodium/iodide symporter: synthesis and biological evaluation *in vitro* and *in vivo*

Alex Khoshnevisan[1], **Krisanat Chuamsaamarkkee**[1], **Mehdi Boudjemeline**[1,†], **Alex Jackson**[2], **Gareth E. Smith**[2], **Antony D. Gee**[1], **Gilbert O. Fruhwirth**[1], and **Philip J. Blower**[1,*]

[1]King's College London, Division of Imaging Sciences and Biomedical Engineering, 4th Floor Lambeth Wing, St. Thomas' Hospital, London SE1 7EH, United Kingdom

[2]GE Healthcare, The Grove Centre, White Lion Road, Amersham, United Kingdom

Abstract

Purpose—Anion transport and accumulation by the human sodium/iodide symporter (hNIS) is an established target for molecular imaging and radionuclide therapy. Current radiotracers for PET imaging of hNIS expression are limited to [^{124}I]I^- and [^{18}F]BF_4^-. We sought to develop new ^{18}F-labeled hNIS substrates offering higher specific activity, higher affinity and simpler radiochemical synthesis than [^{18}F]BF_4^-.

Methods—The ability of a range of anions, some containing fluorine, to block [^{99m}Tc]TcO_4^- uptake in a hNIS-expressing cell line was measured. SO_3F^- emerged as a promising candidate. [^{18}F]SO_3F^- was synthesised by reaction of [^{18}F]F^- with SO_3-pyridine complex in MeCN and purified using alumina and QMA SPE cartridges. Chemical and radiochemical purity and stability in human serum were determined by radiochromatography. Radiotracer uptake and efflux in hNIS-transduced HCT116-C19 cells and the hNIS-negative parent cell line were evaluated *in vitro* in the presence and absence of a known substrate ($NaClO_4$) as a competitive inhibitor. PET/CT imaging and *ex vivo* biodistribution measurement were conducted in Balb/c mice, both with and without $NaClO_4$ inhibition.

[*]**Corresponding Author Details**: Prof. Philip J. Blower; Address: King's College London, Division of Imaging Sciences and Biomedical Engineering, 4th Floor Lambeth Wing, St. Thomas' Hospital, London SE1 7EH, United Kingdom; Tel: 02071889513; philip.blower@kcl.ac.uk.

First Author Details

Mr. Alex Khoshnevisan; Address: King's College London, Division of Imaging Sciences and Biomedical Engineering, 4th Floor Lambeth Wing, St. Thomas' Hospital, London SE1 7EH, United Kingdom; Tel: 02071888376; Email: alex.khoshnevisan@kcl.ac.uk, PhD Student

[†]Current address: McGill University, McConnell Brain Imaging Centre, Montreal Neurological Institute, Montreal H3A 2B4, Canada

Disclosure

AK and PJB have filed a patent relating to the material in this publication. The other authors declare that they have no competing interests.

Authors Contributions

PJB conceived the study, secured funding and contributed to its design and coordination. GOF and MB contributed data on pertechnetate uptake inhibition. AK developed the fluorosulfate radiolabeling and radioanalytical methods, and performed *in vitro* and serum stability studies. KC and AK performed the *in vivo* experiments. KC performed the image analysis and quantification. AJ, GS and ADG contributed to study design. The manuscript was drafted by AK and PJB and edited by all other authors. All authors have read and approved the final manuscript.

Results—The fluorosulfate anion was identified as a potent inhibitor of [^{99m}Tc]TcO_4^- uptake via hNIS *in vitro* (IC_{50} 0.55-0.56 μM, cf. BF_4^- 0.29-4.5, TcO_4^- 0.07, I^- 2.7-4.7 μM). Radiolabeling to produce [^{18}F]SO_3F^- was simple to perform and afforded the desired radiotracer in high radiochemical purity, suitable for biological evaluation (RCP > 95%, decay corrected RCY = 31.6%, specific activity ≥ 48.5 GBq/μmol). Specific, blockable hNIS-mediated uptake in HCT116-C19 cells was observed *in vitro,* and PET/CT imaging in normal mice showed uptake in thyroid, salivary glands (%ID/g at 30 min: 563 ± 140 and 32 ± 9 respectively) and stomach (%ID/g at 90 min: 68 ± 21).

Conclusions—Fluorosulfate is a high-affinity hNIS substrate. [^{18}F]SO_3F^- is easily synthesized in high yield and very high specific activity and is a promising candidate for pre-clinical and clinical PET imaging of hNIS expression and thyroid-related disease; it is the first example of *in vivo* PET imaging with a tracer containing a S-^{18}F bond.

Keywords

Human sodium/iodide symporter (SC5A5); fluorosulfate; fluorine-18; PET; thyroid

Introduction

The sodium/iodide symporter (NIS) is capable of intracellular concentration of certain small anions against their electrochemical gradient, and has an important biological role in accumulating iodide in thyroid follicles as a substrate for synthesis of thyroid hormones. Several radioactive substrates of human NIS (hNIS; SC5A5) have been used effectively for radionuclide therapy ([^{131}I]I^-) and SPECT ([$^{131/123}$I]I^-, [^{99m}Tc]TcO_4^-) and PET ([^{124}I]I^-) imaging applications of thyroid-related disorders (1). Other radioactive substrates currently being evaluated as potential next-generation radiopharmaceuticals for these purposes include [$^{186/188}$Re]ReO_4^- for therapy (2,3) and [^{18}F]BF_4^- for PET (4,5). [^{18}F]BF_4^- is the prototype ^{18}F-labeled NIS tracer and offers all the advantages associated with fluorine-18: moderate half life, excellent imaging characteristics associated with a high yield of low-energy positrons, minimal undesirable photon emissions, low absorbed radiation dose and potentially wide availability. As a result of these characteristics, it is expected to offer superior imaging compared to SPECT with $^{123/131}$I and PET with ^{124}I. However, among the known substrates of NIS it has mid-ranking affinity with an IC_{50} of 1.2 μM for inhibition of [^{124}I]I^- uptake (c.f. IC_{50} of ClO_4^- is 0.1 μM in the same assay (6)), and chemical constraints during synthesis lead to low specific activity (4,7). Consequently, alternative fluorine-18-labeled NIS substrates that overcome these limitations are desirable.

A search of the literature for alternative fluorine-containing NIS substrates reveals several that merit further investigation. Both SO_3F^- and $PO_2F_2^-$ are known to inhibit radioiodide uptake in mouse thyroid (8), yet in quantitative terms their effectiveness as substrates or inhibitors of hNIS is unknown. PF_6^- has previously been shown to be a highly potent inhibitor of rat NIS (IC_{50} = 15 nM (9)). We therefore performed a preliminary comparison of their ability to inhibit hNIS using uptake in hNIS expressing cells with [^{99m}Tc]pertechnetate as a probe. From this initial survey we selected SO_3F^- as a candidate offering both high affinity and the possibility of straightforward radiolabeling.

Europe PMC Funders Author Manuscripts

Here we report a comparison of fluorine-containing anions with other known hNIS substrates and, for the first time, a simple method for radiosynthesis of $[^{18}F]SO_3F^-$ together with its biological evaluation in hNIS-expressing cells and *in vivo* in mice.

Materials and Methods

General

Unless otherwise stated, all reagents and materials were purchased from Sigma Aldrich (Gillingham, UK). Ammonium difluorophosphate was synthesized using a method adapted from that of Lange et al. (10) (details in Supplementary Information (SI)). $[^{18}F]F^-$ was produced by proton irradiation of $[^{18}O]H_2O$ (Rotem Industries Ltd., Israel, 98 atom %) using a CTI 11 MeV RDS 112 cyclotron. $[^{99m}Tc]TcO_4^-$ was obtained from Guy's Hospital Radiopharmacy (London, UK) and used ~4.5 h after generator elution and an elapsed time of 24 h between each consecutive elution. Animal experiments were performed under a UK Home Office licence in accordance with UK Research Councils' and Medical Research Charities' guidance on Responsibility in the Use of Animals in Bioscience Research, and approved by the local institutional ethics committee. For assessment of inhibitory potency by pertechnetate uptake blockade, we used two different cell lines expressing hNIS: (i) a breast adenocarcinoma cell line that was virally infected and stably expresses hNIS (11): MTLn3E.Δ34 CXCR4-eGFP hNIS-tag-RFP cells, hereafter referred to as 3E.Δ-NIS cells), and (ii) a human colon carcinoma cell line that was transfected to stably express hNIS under selection pressure (HCT116-hNIS-C19 (5)). Parental cell lines served as negative controls. HCT116 was also used also to study the cellular uptake of $[^{18}F]SO_3F^-$ in the absence of hNIS. Details of the pertechnetate uptake blockade experiments are given in SI. Ionic volumes were either taken directly from data by Jenkins et al. (12), or calculated by the method described therein from crystallographic data. For $PO_2F_2^-$, crystallographic data from Trotter and Whitlow (13) were used. For TcO_4^- crystallographic data from McDonald and Tyson(14), and Krebs and Hasse (15) were used. Details of radiochemistry development, radioanalytical methods, other analytical methods, *in vitro* experiments assessing the biological behaviour of $[^{18}F]SO_3F^-$ and stability studies are given in SI.

Optimized radiosynthesis

Solutions of K_2CO_3 (5.2 mg) in H_2O (0.4 mL) and of K[2.2.2] (14.2 mg) in MeCN (1.1 mL) were prepared. A portion of the K_2CO_3 solution (0.2 mL) was then added to the K[2.2.2] solution to form the QMA eluent. $[^{18}F]$fluoride was trapped by passing irradiated H_2O over a QMA cartridge (preconditioned $NaHCO_3$ (10 mL), H_2O (10 mL)), and then eluted with the QMA eluent (0.9 mL). The fluoride was dried by azeotropic distillation under a N_2 stream, first at 110°C for 5 min, then twice further at 95°C with addition of MeCN (0.4 mL) each time. SO_3-pyridine complex (5 mg) in MeCN (1 mL) was then added to the dried residue followed by heating to 80°C for 10 min. The reaction was then quenched by addition of H_2O (2 mL) and the solution passed through a neutral alumina cartridge (preconditioned with H_2O (20 mL) and air (10 mL)) and a QMA cartridge (preconditioned 1M NaCl (5 mL), H_2O (10 mL)). The QMA was washed with H_2O (4 mL) and the product was then eluted with 0.9% NaCl (0.4 mL) ready for biological evaluation.

PET imaging

Female Balb/c mice (4 - 8 weeks of age) were injected with either $NaClO_4$ (intraperitoneal injection as a competitive substrate for inhibitive effect in 0.9% NaCl, 250 mg/kg) or an equal volume of 0.9% NaCl (sham inhibitor) 1 h prior to commencement of scanning. [^{18}F]SO_3F^- (~5 MBq in 0.9% NaCl, 150 μL) was then injected intravenously (tail vein) under anesthesia maintained using 1.5 - 2% isoflurane gas (Isocare®, in O_2 (Animalcare, York, UK)). The mouse was then transferred to the scanner bed where anesthesia, bed warming and vital signs monitoring were maintained. Dynamic PET was continuously acquired for 2 h (starting < 1 min after tracer injection) on the nanoScan-PET/CT (Mediso, Hungary) in list mode using 400-600 keV energy window and coincidence relation of 1:3 followed by CT (55 keV X-ray, exposure time 1000 ms and 360 projections and pitch 1). All PET projection data were processed with the 3D reconstruction Tera-tomo® software package (supplied with the system) with attenuation, scatter and dead-time corrections. Data were re-binned and reconstructed into a series of 5 min time frames for the first 30 min and then 30 min time frames for the remaining scan period. The VivoQuant© (InviCro, Boston, USA) software was used to view and quantify the data. Regions of interest (ROIs) were manually drawn over the thyroid, salivary glands, stomach, bladder, left ventricle (for blood), and muscle at a threshold of 10% of the maximum count to define the edges of the ROI. The CT images were used as a guide to resolve areas not clear from the radionuclide images. Time-activity curves were generated and expressed as percentage injected dose (%ID, taking the whole body ROI activity, excluding tail, as the injected dose) and percentage injected dose per *ex vivo* weight of organ (%ID/g).

Ex vivo biodistribution

At 2.25 h post-injection, after completion of the above scanning protocol, mice were culled by cervical dislocation and tissues were harvested for *ex vivo* biodistribution. Thyroid was dissected under a microscope. All tissues were then weighed and counted using a gamma counter (1282 Compugamma; LKB, window set to channels 175-220). *Ex vivo* biodistribution data were presented as %ID/g where ID represents the sum of the activity of all body parts including carcass, and including any urine excreted at the time of culling, but excluding the tail. Calculations requiring thyroid weight were conducted using a standard weight of 3.6 mg (4,16) owing to potential inaccuracies in dissection and weighing introduced by its small size.

Results

$^{99m}TcO_4^-$ uptake inhibition assay

The half-maximal inhibitory concentrations (IC_{50}) for the anions assessed for their ability to block [^{99m}Tc]TcO_4^- or [^{18}F]BF_4^- uptake via hNIS are detailed in SI (Table S1, which also includes comparable literature data (5,6,7,9,17). The potency of the anions was found to be in the order $SCN^- < PO_2F_2^- < I^- < BF_4^- \approx SO_3F^- < ReO_4^- < TcO_4^- < PF_6^-$: a trend which roughly parallels the increase in ionic volume (Fig. 1). Literature data on inhibitory potency and affinity of anions are not comprehensive but our data are broadly consistent with previous results where available. Of the fluorine-containing substrates examined, PF_6^- (IC_{50} 21 nM) was the most potent but SO_3F^- had potency (IC_{50} 0.56 mM) comparable to BF_4^- and

better than iodide (IC_{50} >2.7 mM), and is more likely to be amenable to simple radiosynthesis than BF_4^-. The latter was therefore selected as the basis for development of a new PET tracer.

Radiosynthesis of $[^{18}F]SO_3F^-$

Reaction of K[2.2.2]/$[^{18}F]$KF with SO_3-pyridine complex (Figure 2) afforded the desired product, $[^{18}F]SO_3F^-$, as confirmed by IC. Varying the reaction conditions (SI Table S2) allowed crude RCY values as high as 65% to be obtained. Passage through an alumina column removed unreacted $[^{18}F]F^-$, and the eluted product could be trapped on a QMA cartridge allowing washing to remove chemical impurities (pyridine and K[2.2.2]). The final product could be eluted in 0.9% NaCl with a radiochemical yield (RCY) of 31.6 ± 9.5% (n = 3, decay corrected) and radiochemical purity (RCP) greater than 95%. The total synthesis time from trapping precursor fluoride to elution of final product was less than 1 hour. The identity of the product was confirmed by ion chromatography with co-injection of authentic SO_3F^- as a reference (Figure 3). With a starting radioactivity of ~750 MBq, a specific activity of ≥ 48.5 ± 13.4 GBq/μmol (n = 3) was obtained in a volume of 0.4 mL. The concentration of pyridine in the product was 1.4 ± 1 μg/mL (0.56 μg total); that of K[2.2.2] was < 6.25 μg/mL (< 2.5 μg total); and that of SO_4^{2-} was 302 ± 26 μg/mL (120.7 μg total). The final formulation was clear and colourless with a pH of 7.

In vitro uptake, efflux and self-inhibition of $[^{18}F]SO_3F^-$

Significant uptake of the radiotracer in hNIS-expressing HCT116-C19 cells was observed and could be blocked by addition of $NaClO_4$ (Figure 4). No uptake was observed in the parental cell line HCT116 (which does not express hNIS), either in the presence or absence of $NaClO_4$. Uptake of the tracer over time, and efflux of the tracer from the cell were both found to reach equilibrium within 80 min (SI Figures S3 and S4, respectively). The uptake at equilibrium is consistent with an intracellular-to-extracellular $[^{18}F]SO_3F^-$ concentration ratio of 76:1. For comparison, under identical conditions the ratio for $[^{99m}Tc]TcO_4^-$ was 44:1, and that for $[^{18}F]BF_4^-$ was 24:1, calculated from data obtained during this study, and other studies (7) respectively. Inhibition of $[^{18}F]SO_3F^-$ uptake in HCT116-C19 cells by KSO_3F was observed with an IC_{50} of 1.6 μM (Figure 5).

Serum stability

IC and TLC after allowing the formulated tracer to stand at room temperature for 4 h indicated that it was stable and maintained an RCP > 95%. The RCP of the tracer was similarly constant over a 4 h period under acidic conditions (pH 3.0). Incubation with human serum yielded similar results, with the RCP of the tracer remaining > 95% over a 4 h period as assessed by TLC of the supernatant after protein precipitation with ethanol (no significant radioactivity was associated with the protein pellet). These data are summarised in SI Table 3.

PET/CT imaging

Imaging the biodistribution of $[^{18}F]SO_3F^-$ by PET/CT (Figure 6) in normal mice revealed prominent uptake in the thyroid, stomach and salivary glands, that was suppressed in the

perchlorate-treated mice. Time-activity curves (SI Figure 5 and 6) illustrating the %ID/g (%ID data shown in SI Figure 7 and 8) present in NIS-expressing organs and bladder over a 2 h imaging period showed thyroid and salivary gland uptake reaching a plateau around 30-45 min (563 ± 140 and 32 ± 9 %ID/g at 30 min respectively), with stomach uptake plateauing around 90 min (68 ± 21 %ID/g at 90 min). Bone uptake first became detectable at 30 min and increased by the 60 min time point (3 ± 1 %ID/g at 60 min).

Ex vivo biodistribution in mice

At 2.25 h post-injection, significant uptake of $[^{18}F]SO_3F^-$ consistent with the PET scans was observed in the thyroid (144 ± 71 %ID/g), stomach (59 ± 10 %ID/g) and salivary glands (18 ± 4 %ID/g), whereas uptake in these organs was blocked (reduced to 4.3 ± 4.6, 3.0 ± 1.7 and 2.6 ± 1.7 %ID/g respectively) in mice administered with a known NIS inhibitor, $NaClO_4$ (Figure 6, shown as SUV in SI Figure 9). The magnitude of the radioactivity observed in the bladder (15 ± 14 %ID/g) indicates that the tracer is excreted via the renal route. A small amount of radioactivity uptake in bone (17 ± 3 %ID/g) was observed and was not blocked by perchlorate, suggesting that some defluorination occurs over the two hour time period that was not seen during incubation in serum.

Discussion

Evaluation of the inhibitory potency of fluorosulfate on hNIS both confirmed its previously-suggested (8) status as a potent NIS inhibitor/competitive substrate, and estimated it to be more potent than I^- and possibly BF_4^-. The range of IC_{50} values found here for both BF_4^-, which is currently undergoing evaluation as a clinical PET tracer for hNIS, and SO_3F^- is lower than the range of values found for iodide (Figure 1 and SI Table S1). Although inhibitory potency may not be directly indicative of ability to reach a high intracellular-extracellular concentration gradient in hNIS expressing cells (which is the key requirement of a good PET tracer for hNIS), it is a reasonable indicator that SO_3F^- may form the basis of a high affinity PET tracer for NIS. Analysis of the ionic volume (12) in relation to the IC_{50} of several anions against radioiodide (9), $[^{99m}Tc]TcO_4^-$ or $[^{18}F]BF_4^-$ uptake suggests a trend wherein larger anionic species appear to be more effective inhibitors of hNIS (Figure 1). In keeping with this trend, PF_6^- was found to be the most potent inhibitor examined (IC_{50} 21 nM). However, in contrast to other known fluorine-containing NIS inhibitors such as PF_6^- and BF_4^-, SO_3F^- has the advantage of bearing a single fluorine atom. This is significant; any no-carrier-added radiolabeling of SO_3F^- would yield a product with a specific activity limited only by the fluorine-18 source. These factors led to a selection of $[^{18}F]SO_3F^-$ as a target for development of a new fluorine-18-labeled hNIS tracer.

Our radiosynthetic strategy for synthesising $[^{18}F]SO_3F^-$ involved utilizing a Lewis acid-base sulfur trioxide-pyridine adduct, which is readily available as a pure, high quality starting material. Radiolabeling proceeded via displacement of the pyridine by $[^{18}F]F^-$ followed by quenching with water to hydrolyse residual starting material to sulfate. Formation of $[^{18}F]SO_3F^-$, confirmed by TLC and IC, was observed under all reaction conditions examined. Varying the reaction conditions suggested that more basic conditions with elevated temperature and precursor concentration could enhance the incorporation of $[^{18}F]F^-$

into $[^{18}F]SO_3F^-$. Further optimization may in future lead to improved incorporation of $[^{18}F]F^-$ into the final product, e.g. using alternatives to pyridine as the Lewis base in the precursor complex.

Purification using sequential alumina and quaternary ammonium cartridges yielded $[^{18}F]SO_3F^-$ in saline, a medium suitable for biological use, with high radiochemical and chemical purity. The levels of pyridine and K[2.2.2] present in the final product are within the acceptance limits set out in the British Pharmacopoeia and would likely be subject to further dilution in the preparation of a dose for use *in vivo.* The sulfate concentration resulting from precursor hydrolysis upon reaction quenching is also safe considering that $MgSO_4$ can be administered in gram quantities intravenously with minimal side effects (18). The specific activity of $[^{18}F]SO_3F^-$ (≥ 48.5 GBq/μmol) is significantly higher than that reported for $[^{18}F]BF_4^-$ (1 (4) or 5 (7) GBq/μmol depending on production method) as there is no ^{19}F naturally present in the precursor. The specific activity is therefore limited only by that of the initial $[^{18}F]F^-$ and the purity of the other reagents. The production method is amenable to automation and taken with the safe levels of potential chemical contaminants reported here, modification of the radiosynthesis to conform to Good Manufacturing Practices should be a straightforward task. The high specific activity minimizes the pharmacological dose administered, allowing the radioactivity dose to be optimal.

Assessing the biological activity of $[^{18}F]SO_3F^-$ *in vitro* in a hNIS-expressing cell line confirmed specific NIS-mediated uptake that was absent both in hNIS-negative cells and in the presence of competitive inhibition by a known substrate, perchlorate. Time-dependant analysis of uptake and efflux showed kinetics (equilibrium reached in under 80 min) appropriate for *in vivo* use. The specific activity of the $[^{18}F]SO_3F^-$ is very high and more than sufficient to realise the potential benefit of the high affinity: assuming an injected amount of ~10 MBq for a PET/CT scan in a mouse with an extracellular fluid volume of 5 mL, the *in vivo* concentration of $[^{18/19}F]SO_3F^-$ will be no more than 41 nM. This is well below the concentration range at which *in vitro* inhibition is observed (Figure 5). As well as a high affinity of $[^{18}F]SO_3F^-$ for hNIS demonstrated by the IC_{50} value of 0.56 μM, the intracellular-to-extracellular radioactivity concentration ratio achieved at the plateau of uptake in the *in vitro* cell uptake studies (76:1) was higher than for either $[^{99m}Tc]$pertechetate (44:1) or $[^{18}F]BF_4^-$ (24:1), suggesting that, other pharmacokinetic features being similar, a higher target-to-background ratio might be expected in PET images.

PET/CT imaging of $[^{18}F]SO_3F^-$ in normal mouse models during the first hour post-injection revealed uptake at sites known to express NIS endogenously, in addition to clearance via the renal route. This signal was abolished by co-administration of a known NIS substrate, $NaClO_4$. This shows that the tracer is an excellent substrate for mouse NIS as well as hNIS. Maxima were reached in both the thyroid uptake (SI Figure S5) and the ratio of thyroid to muscle (as a background reference) uptake (SI Figure S10) after 30 min, confirming this as the ideal imaging time point. While barely detectable at 30 min (%ID/g <1% of that in thyroid), there was increasing signal in the bones at later time points, as observed both in later PET images and in the *ex vivo* biodistribution data. While the *in vivo* hydrolysis of fluorosulfate to sulfate and fluoride is known (19), it is unlikely to hamper the utility of the

tracer in hNIS imaging applications because uptake of the tracer at sites of NIS expression reaches its maximum long before bone uptake is significant.

Conclusion

Several fluorine-containing anions are potent hNIS inhibitors. Among them SO_3F^- is a hNIS inhibitor containing a single fluorine atom that has an inhibitory potency in the same order or greater than that of tetrafluoroborate, and greater than iodide. It is readily synthesized in fluorine-18-radiolabeled form by a simple method in high yield, radiochemical purity and specific activity. $[^{18}F]SO_3F^-$ shows NIS-specific uptake *in vitro* and *in vivo* and is an excellent candidate for further preclinical and clinical evaluations as a hNIS PET imaging agent with potential for application in thyroid-related disease and hNIS reporter gene imaging. To our knowledge, this work is the first example of S-^{18}F bond imaging *in vivo* by PET/CT. The simplicity of the synthesis of $[^{18}F]SO_3F^-$, and its adequate *in vivo* stability, suggest that the "inorganic" approach to ^{18}F-radiopharmaceutical synthesis (20) whereby atoms other than carbon, such as aluminum, silicon, boron, and now sulfur (21), can serve as a binding site for ^{18}F, deserves further attention.

Supplementary Material

Refer to Web version on PubMed Central for supplementary material.

Acknowledgements

This work was supported by an EPSRC Industrial CASE studentship awarded to GE Healthcare and King's College London; the Biomedical Research Centre award to Guy's & St Thomas' NHS Foundation Trust in partnership with King's College London and King's College Hospital NHS Foundation Trust; an MRC Confidence in Concept Award administered by King's Health Partners; the Centre of Excellence in Medical Engineering funded by the Wellcome Trust and EPSRC under grant number WT088641/Z/09/Z; and the King's College London and UCL Comprehensive Cancer Imaging Centre funded by the CRUK and EPSRC in association with the MRC and DoH (England). The views expressed are those of the author(s) and not necessarily those of the NHS, the NIHR or the DoH. PET scanning equipment was funded by an equipment grant from the Wellcome Trust.

References

1. Ahn B-C. Sodium iodide symporter for nuclear molecular imaging and gene therapy: from bedside to bench and back. Theranostics. 2012; 2:392–402. [PubMed: 22539935]
2. Riese CGU, Seitz S, Schipper ML, Behr TM. Effective treatment of pancreatic neuroendocrine tumours transfected with the sodium iodide symporter gene by ^{186}Reperrhenate in mice. Eur J Nucl Med Mol Imaging. 2009; 36:1767–73. [PubMed: 19449003]
3. Dadachova E, Bouzahzah B, Zuckier LS, Pestell RG. Rhenium-188 as an alternative to iodine-131 for treatment of breast tumors expressing the sodium/iodide symporter (NIS). Nucl Med Biol. 2002; 29:13–8. [PubMed: 11786271]
4. Jauregui-Osoro M, Sunassee K, Weeks AJ, Berry DJ, Paul RL, Cleij M, et al. Synthesis and biological evaluation of [^{18}F]tetrafluoroborate: a PET imaging agent for thyroid disease and reporter gene imaging of the sodium/iodide symporter. Eur J Nucl Med Mol Imaging. 2010; 37:2108–16. [PubMed: 20577737]
5. Weeks AJ, Jauregui-Osoro M, Cleij M, Blower JE, Ballinger JR, Blower PJ. Evaluation of [^{18}F]-tetrafluoroborate as a potential PET imaging agent for the human sodium/iodide symporter in a new colon carcinoma cell line, HCT116, expressing hNIS. Nucl Med Commun. 2011; 32:98–105. [PubMed: 21085047]

6. Tonacchera M, Pinchera A, Dimida A, Ferrarini E, Agretti P, Vitti P, et al. Relative potencies and additivity of perchlorate, thiocyanate, nitrate, and iodide on the inhibition of radioactive iodide uptake by the human sodium iodide symporter. Thyroid. 2004; 14:1012–9. [PubMed: 15650353]
7. Khoshnevisan A, Jauregui-Osoro M, Shaw K, Baguna Torres J, Young JD, Ramakrishnan NK, et al. [^{18}F]tetrafluoroborate as a PET tracer for the sodium/iodide symporter: the importance of specific activity. EJNMMI Res. 2016; 6:34. [PubMed: 27103614]
8. Anbar M, Guttmann S, Lewitus Z. Effect of monofluorosulphonate, difluorophosphate and fluoroborate ions on the iodine uptake of the thyroid gland. Nature. 1959; 183:1517–8. [PubMed: 13666792]
9. Waltz F, Pillette L, Ambroise Y. A nonradioactive iodide uptake assay for sodium iodide symporter function. Anal Biochem. 2010; 396:91–5. [PubMed: 19733144]
10. Lange W, Booth HS, Kendall F. Ammonium DifluophosphateInorg Synth. Fernelius WC, editorJohn Wiley & Sons, Inc.; 1946. 157–8.
11. Fruhwirth GO, Diocou S, Blower PJ, Ng T, Mullen GED. A whole-body dual-modality radionuclide optical strategy for preclinical imaging of metastasis and heterogeneous treatment response in different microenvironments. J Nucl Med. 2014; 55:686–94. [PubMed: 24604910]
12. Jenkins HDB, Roobottom HK, Passmore J, Glasser L. Relationships among ionic lattice energies, molecular (formula unit) volumes, and thermochemical radii. Inorg Chem. 1999; 38:3609–20. [PubMed: 11671116]
13. Trotter J, Whitlow SH. The structures of cæsium and rubidium difluorophosphates. J Chem Soc Inorg Phys Theor. 1967:1383–6.
14. McDonald BJ, Tyson GJ. The crystal structure of caesium, ammonium and potassium pertechnetates. Acta Crystallogr. 1962; 15:87.
15. Krebs B, Hasse KD. Refinements of the crystal structures of KTcO4, KReO4 and OsO4. The bond lengths in tetrahedral oxoanions and oxides of d^0 transition metals. Acta Crystallogr B. 1976; 32:1334–7.
16. Rugh R. The mouse thyroid and radioactive iodine (I-131). J Morphol. 1951; 89:323–65.
17. Lecat-Guillet N, Ambroise Y. Discovery of Aryltrifluoroborates as Potent Sodium/Iodide Symporter (NIS) Inhibitors. ChemMedChem. 2008; 3:1207–9. [PubMed: 18470860]
18. Demirkaya Ş, Vural O, Dora B, Topçuoğlu MA. Efficacy of intravenous magnesium sulfate in the treatment of acute migraine attacks. Headache J Head Face Pain. 2001; 41:171–7.
19. Mendrala AL, Markham DA, Eisenbrandt DL. Rapid Uptake, Metabolism, and Elimination of Inhaled Sulfuryl Fluoride Fumigant by Rats. Toxicol Sci. 2005; 86:239–47. [PubMed: 15888664]
20. Smith GE, Sladen HL, Biagini SCG, Blower PJ. Inorganic approaches for radiolabelling biomolecules with fluorine-18 for imaging with positron emission tomography. Dalton Trans. 2011; 40:6196–205. [PubMed: 21499604]
21. Inkster JAH, Liu K, Ait-Mohand S, Schaffer P, Guérin B, Ruth TJ, et al. Sulfonyl Fluoride-Based Prosthetic Compounds as Potential 18F Labelling Agents. Chem Eur J. 2012; 18:11079–87. [PubMed: 22807282]

Europe PMC Funders Author Manuscripts

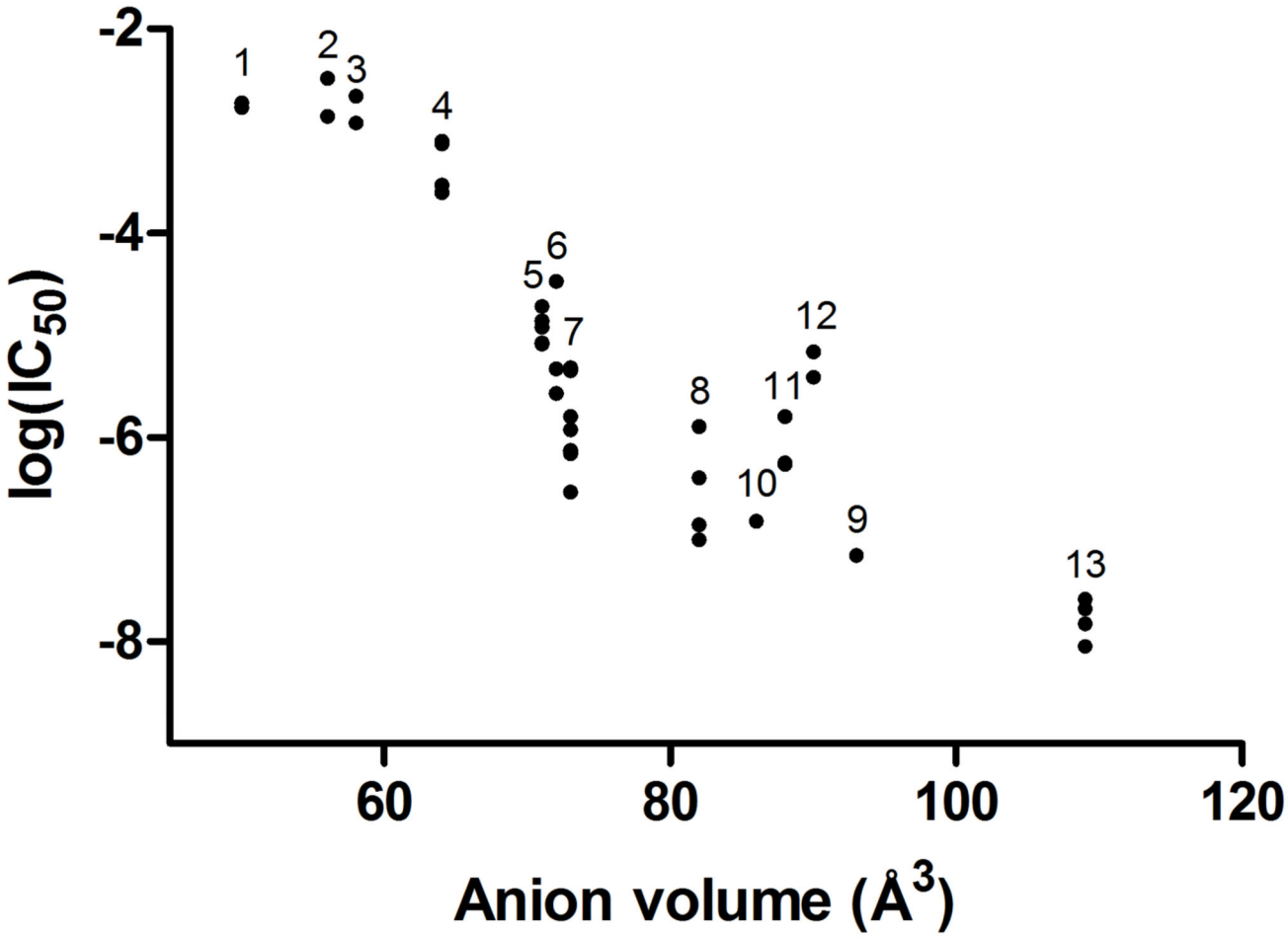

Figure 1.

Plot of ionic volume against inhibitory potency ($logIC_{50}$ based on ability to block anion uptake in NIS-expressing cells) for univalent anions examined in this work and other published works (5,6,7,9,17). Differing methods, cell lines, probes and counter-ions were used in each study; further details are given in SI Table S1. Numeric labels above each column of data points correspond to particular anions: 1 = CN^-, 2 = Br^-, 3 = N_3^-, 4 = NO_3^-, 5 = SCN^-, 6 = I^-, 7 = BF_4^-, 8 = ClO_4^-, 9 = TcO_4^-, 10 = ReO_4^-, 11 = SO_3F^-, 12 = $PO_2F_2^-$, 13 = PF_6^-

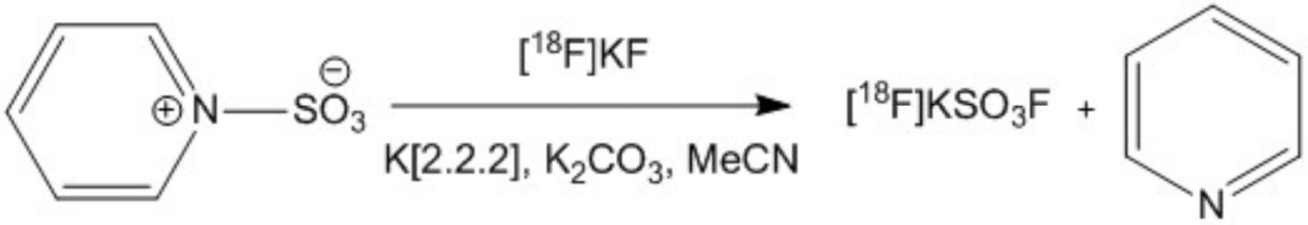

Figure 2.
Reaction scheme for production of $[^{18}F]SO_3F^-$ from SO_3-pyridine complex

Europe PMC Funders Author Manuscripts

Europe PMC Funders Author Manuscripts

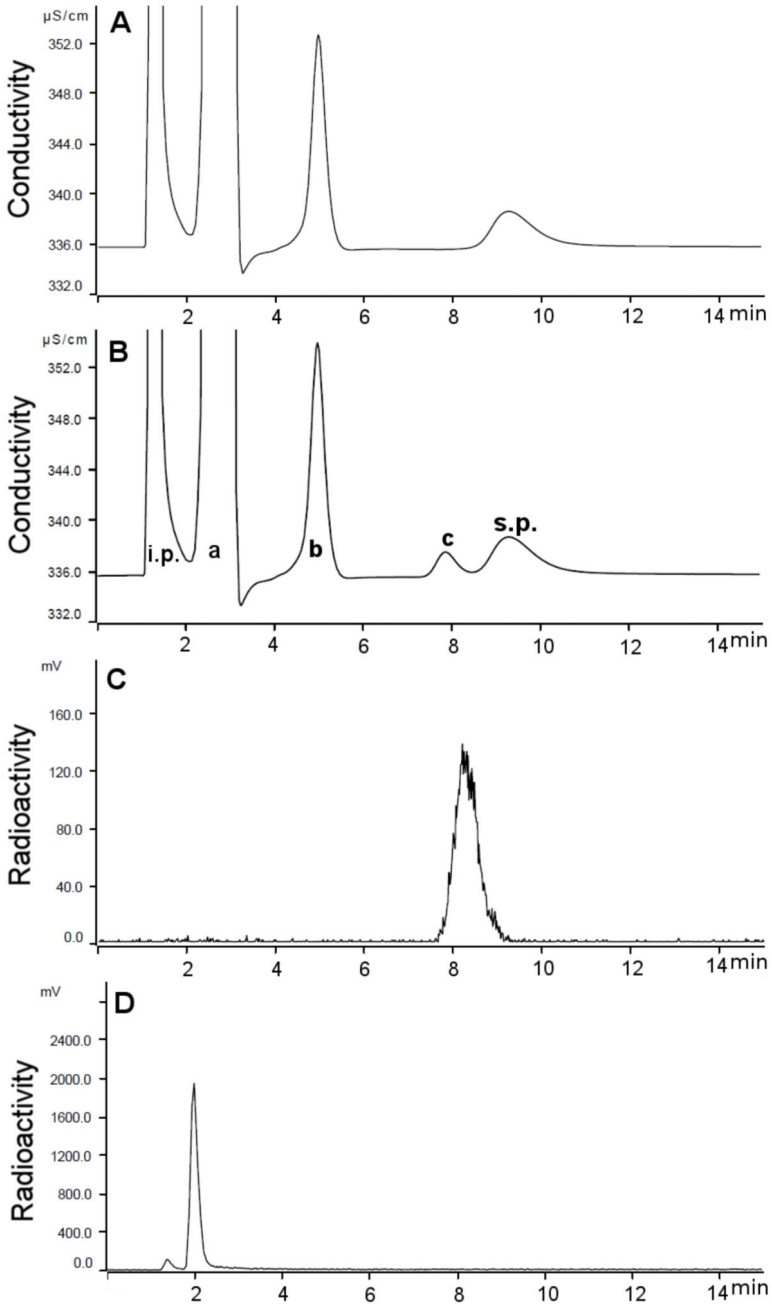

Figure 3.

Chromatograms resulting from IC analysis of $[^{18}F]SO_3F^-$: A – Conductivity trace for no carrier added $[^{18}F]SO_3F^-$; B – Conductivity trace for co-injection of $[^{18}F]SO_3F^-$ with $[^{19}F]SO_3F^-$ (80 μg/mL): a = Cl^-, b = SO_4^{2-}, c = SO_3F^-, i.p. = injection peak, s.p. = system peak.; C – Radioactivity trace for no carrier added $[^{18}F]SO_3F^-$; D – Radioactivity trace for $[^{18}F]F^-$ in H_2O.

Europe PMC Funders Author Manuscripts

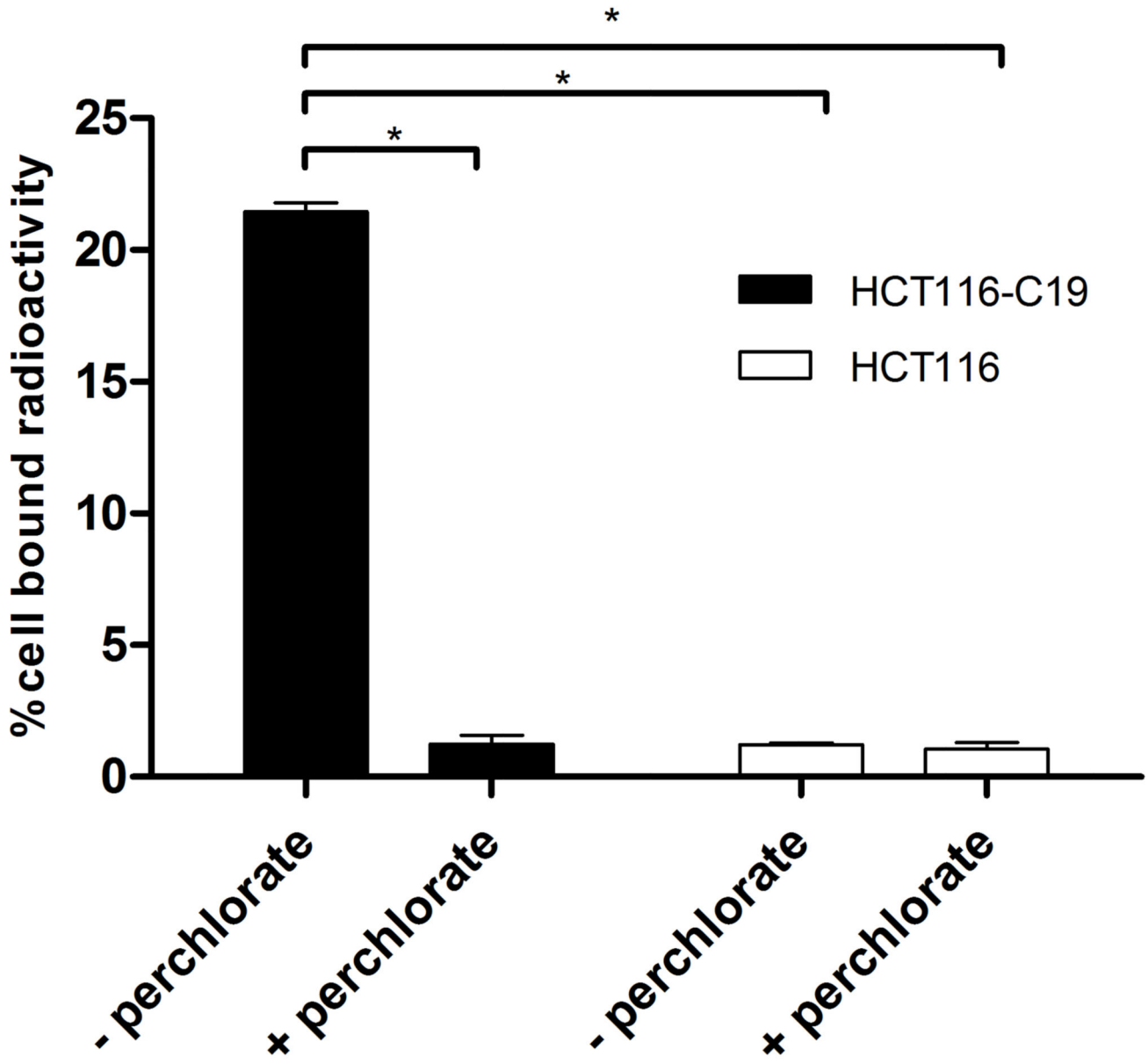

Figure 4.

Uptake of [^{18}F]SO_3F^- in HCT116-C19 (hNIS-expressing) and HCT116 (hNIS-negative) cell lines in the presence and absence of $NaClO_4$ (20 μM). Error bars represent one SD. Inter-group differences measured by unpaired t-test, * $p < 0.00001$.

Europe PMC Funders Author Manuscripts

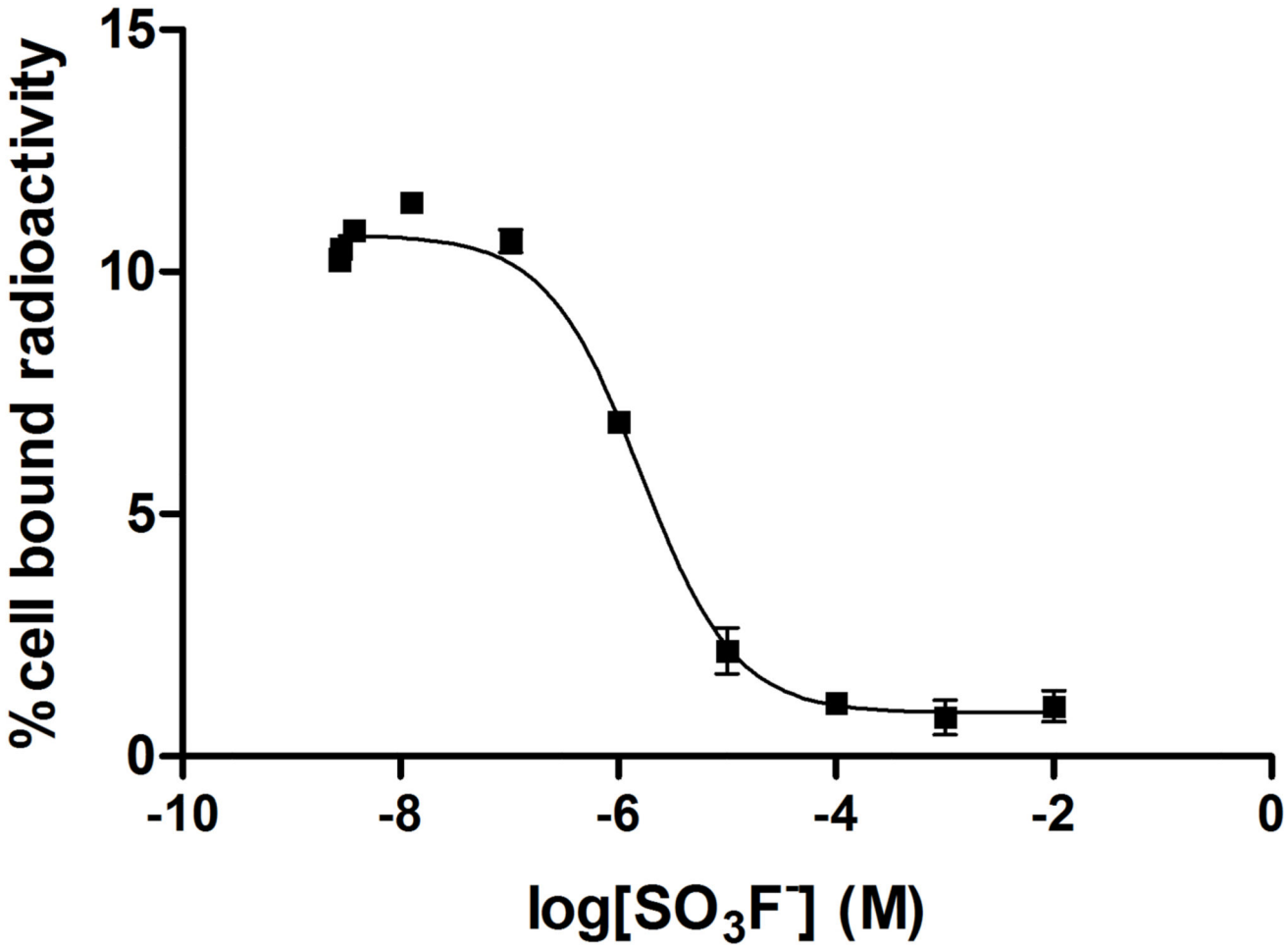

Figure 5.

Inhibition of uptake of $[^{18}F]SO_3F^-$ by $[^{19}F]SO_3F^-$ in HCT116-C19 cells. Error bars represent 1 S.D.; IC_{50} = 1.6 μM

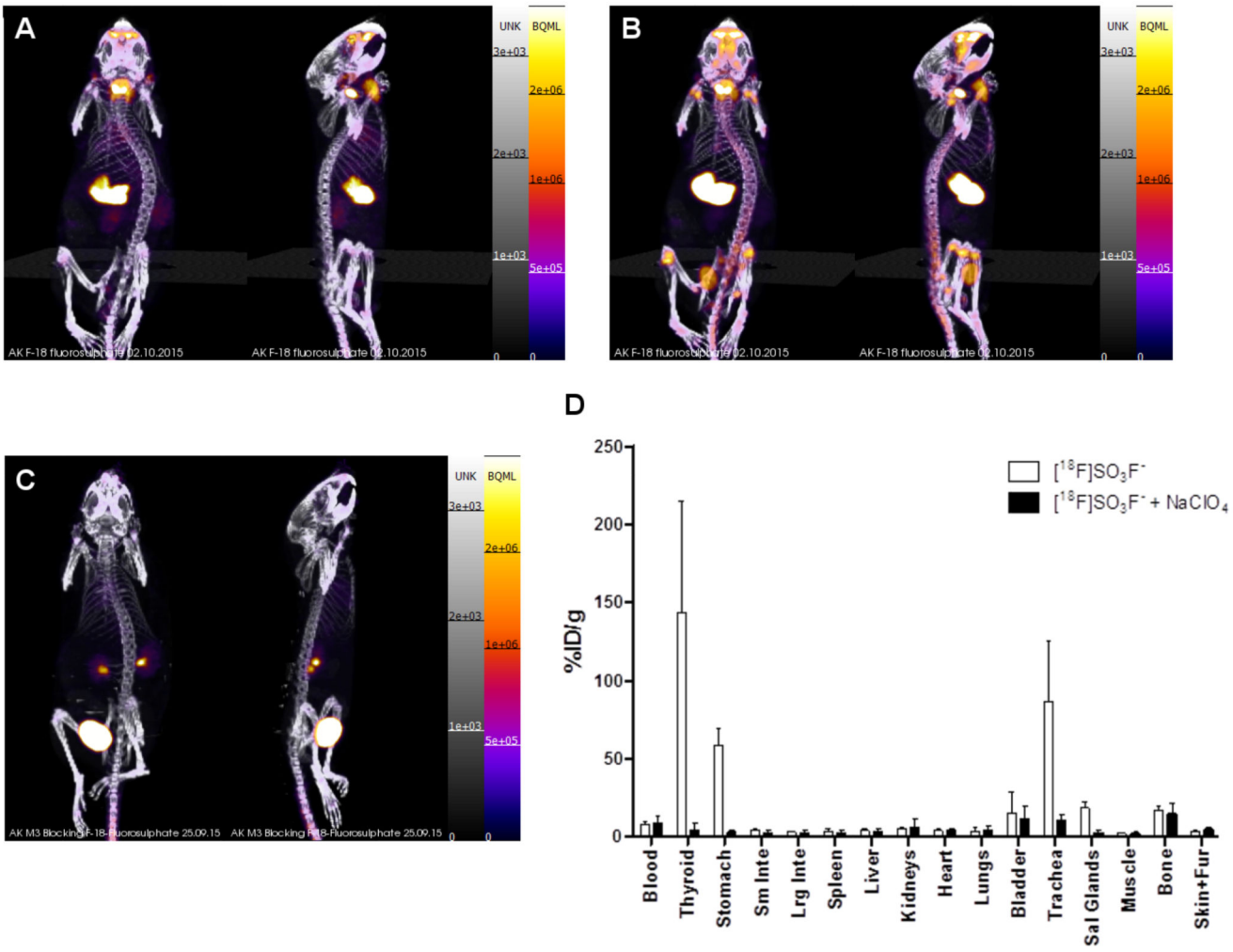

Figure 6.

PET/CT images (maximum intensity projections) from anterior and lateral perspectives (A-C) and *ex vivo* biodistribution (D) of Balb/c mice post-injection of $[^{18}F]SO_3F^-$. A: 25-30 min post-injection without perchlorate; B: 90-120 min post-injection without perchlorate; C: 25-30 min post-injection in the presence of $NaClO_4$ (250 mg/kg); D: *Ex vivo* biodistribution data at 2.25 h post-injection (n = 3). Uptake measured as injected dose per gram (%ID/g). Error bars represent 1 SD.

Europe PMC Funders Author Manuscripts